HHS Public Access

Author manuscript

Exp Eye Res. Author manuscript; available in PMC 2020 August 11.

Published in final edited form as:

Exp Eye Res. 2019 April ; 181: 316–324. doi:10.1016/j.exer.2018.08.019.

Oxidative stress induces ferroptotic cell death in retinal pigment epithelial cells

Kiyohito Totsuka[a,1], **Takashi Ueta**[a,b,1], **Takatoshi Uchida**[a,c], **Murilo F. Roggia**[a], **Suguru Nakagawa**[a], **Demetrios G. Vavvas**[d], **Megumi Honjo**[a], **Makoto Aihara**[a,*]

[a]Department of Ophthalmology, Graduate School of Medicine and Faculty of Medicine, The University of Tokyo, Tokyo, 113-8655, Japan

[b]Department of Ophthalmology, Center Hospital of the National Center for Global Health and Medicine, 1-21-1 Toyama Shinjyuku-ku, Tokyo, 162-8655, Japan

[c]Senju Laboratory, Senju Pharmaceutical Co. Ltd., Kobe, Japan

[d]Angiogenesis Laboratory, Department of Ophthalmology, Massachusetts Eye and Ear, Harvard Medical School, Boston, MA, 02114, USA

Abstract

The dysfunction and cell death of retinal pigment epithelial (RPE) cells are hallmarks of late-stage dry (atrophic) age-related macular degeneration (AMD), for which no effective therapy has yet been developed. Previous studies have indicated that iron accumulation is a source of excess free radical production in RPE, and age-dependent iron accumulation in RPE is accelerated in patients with dry AMD. Although the pathogenic role of oxidative stress in RPE in the development of dry AMD is widely accepted, the mechanisms of oxidative stress-induced RPE cell death remain elusive. Here, we show that ferroptotic cell death, a mode of regulated necrosis mediated by iron and lipid peroxidation, is implicated in oxidative stress-induced RPE cell death *in vitro*. In ARPE-19 cells we observed that the ferroptosis inhibitors ferrostatin-1 and deferoxamine (DFO) rescued *tert*-butyl hydroperoxide (tBH)-induced RPE cell death more effectively than inhibitors of apoptosis or necroptosis. tBH-induced RPE cell death was accompanied by the three characteristics of ferroptotic cell death: lipid peroxidation, glutathione depletion, and ferrous iron accumulation, which were all significantly attenuated by ferrostatin-1 and DFO. Exogenous iron overload enhanced tBH-induced RPE cell death, but this effect was also attenuated by ferrostatin-1 and DFO. Furthermore, mRNA levels of numerous genes known to regulate iron metabolism were observed to be influenced by oxidative stress. Taken together, our observations suggest that multiple modes of cell death are involved in oxidative stress-induced RPE cell death, with ferroptosis playing a particularly important role.

[*]Corresponding author. Department of Ophthalmology, Graduate School of Medicine and Faculty of Medicine, University of Tokyo, Japan, 7-3-1 Hongo Bunkyo, Tokyo, 113-8655, Japan. aihara-tky@umin.net (M. Aihara).

[1]Equally contributed to this study.

Conflicts of interest

All authors declare no competing interests regarding this work.

All authors have approved the final article.

Appendix A. Supplementary data

Supplementary data related to this article can be found at https://doi.org/10.1016/j.exer.2018.08.019.

Keywords

Retinal pigment epithelial cells; Cell death; Oxidative stress; Ferroptosis

1. Introduction

Age-related macular degeneration (AMD), a neurodegenerative disease of the macula, is the leading cause of irreversible central vision loss among the elderly in developed countries (Chou et al., 2016; Wong et al., 2014). The late stage of AMD presents two phenotypes: one is atrophic (or “dry”) AMD, and the other is neovascular (or “wet”) AMD (Miller, 2013). While intravitreal anti-vascular endothelial growth factor (VEGF) therapy has been established for neovascular AMD (Miller, 2010, 2016; Rosenfeld et al., 2005), no effective therapy has yet been developed for atrophic AMD, in which RPE cell dysfunction and cell death are observed (Adler et al., 1999; Bressler et al., 1995; Curcio et al., 2017; Schmitz-Valckenberg et al., 2006; Xu et al., 2017). AMD is a multifactorial disorder caused by aging, genetics, and environmental factors (Evans, 2001; Fritsche et al., 2016; Miller et al., 2017; Thornton et al., 2005). Mechanistically, oxidative stress and free radical damage are believed to contribute to RPE cell death in AMD (Beatty et al., 2000; Hahn et al., 2003; Suzuki et al., 2007; Tate et al., 1995), which has been supported by evidence that oral antioxidant intake prevents or slows the progression of early-stage AMD (Age-Related Eye Disease Study Research Group, 2001).

Recent studies have suggested that iron is implicated in the pathogenesis of AMD as a source of free radicals (Chen et al., 2009; Hahn et al., 2003, 2006). Iron is a biologically essential element that takes part in many processes, including cell proliferation, oxygen transportation, and DNA synthesis. However, excessive iron accumulation can be toxic (Song and Dunaief, 2013). Ferrous iron (Fe^{2+}) catalyzes the conversion of hydrogen peroxide to hydroxyl radicals ($OH^{\bullet}$), the most toxic reactive oxygen species, as well as the conversion of lipid peroxide to lipid alkoxyl radicals ($LO^{\bullet}$) via the Fenton reaction (Halliwell and Gutteridge, 1984). Therefore, intracellular iron levels need to be strictly regulated at the minimum essential levels to avoid oxidative damage. However, retinal iron levels in humans and rats increase with age (Chen et al., 2009; Hahn et al., 2006). In addition, total iron levels in the RPE and Bruch’s membrane are higher in AMD-affected macula compared with age-matched healthy macula (Hahn et al., 2003), and aqueous humor iron levels are elevated more than two fold in patients with dry AMD (Junemann et al., 2013). This supports the hypothesis that oxidative stress and elevated iron levels are implicated in AMD.

While it is accepted that oxidative stress and iron toxicity may be implicated in RPE cell death and the development of AMD, the mechanisms of oxidative stress-induced RPE cell death have not yet been fully elucidated. The majority of previous studies have investigated apoptosis as the mechanism of RPE cell death in response to pro-oxidants such as hydrogen peroxide (H_2O_2) and *tert*-butyl hydroperoxide (tBH), a stable and long-acting form of H_2O_2 (Sharma et al., 2008). Few studies have suggested necrosis as another mechanism for RPE cell death (Kaarniranta et al., 2005; Kim et al., 2003). However, with recent advances in the

understanding of different modes of regulated necrosis (Moreno-Gonzalez et al., 2016), some studies have suggested that necroptosis, a mode of regulated necrosis, is predominantly observed in oxidative stress-induced RPE cell death (Hanus et al., 2013, 2016; Li et al., 2010; Murakami et al., 2014), though other studies have still observed apoptosis (Kim et al., 2010; Yan et al., 2014).

Ferroptosis is a distinct form of regulated necrosis, characterized by lipid peroxidation-induced cell death contingent upon the availability of iron and reactive oxygen species (ROS) (Bertrand, 2017; Cao and Dixon, 2016; Dixon et al., 2012). Ferroptosis is implicated in various pathophysiological states including tumor suppression (Shintoku et al., 2017), neurodegeneration (Do Van et al., 2016), ischemia/reperfusion injury (Friedmann Angeli et al., 2014), and hemochromatosis (Wang et al., 2017). Despite elevated iron levels in the ocular tissues of patients with AMD, the involvement of an iron-dependent mechanism (i.e., ferroptosis) in RPE cell death has not yet been clarified. Here, we show i*n vitro* that, in addition to apoptosis and necroptosis, ferroptotic cell death may be a major mode of oxidative stress-mediated RPE cell death.

2. Materials and methods

2.1. Cell culture

The human retinal pigment epithelial (RPE) cell line ARPE-19 (CRL-2303; ATCC, Manassas, VA, USA) cells were cultured in Dulbecco's modified Eagle's medium with nutrient mixture F-12 (DMEM/F-12) with phenol red (Wako, Tokyo, Japan), supplemented with 10% fetal bovine serum (Sigma-Aldrich, St. Louis, MO, USA), and 1% antibiotic-antimycotic including penicillin, streptomycin, and amphotericin B (Thermo Fisher Scientific, Waltham, MA, USA). The primary human fetal RPE cells (hf-RPE; Lonza, Walkersville, MD, USA) were cultured in RtEGM (Lonza, Basel, Switzerland) supplemented with 2% L-glutamine (Lonza), 0.5% FGF-B (Lonza), and 0.25% GA (Lonza). ARPE-19 and hf-RPE cells were used between passages 2 and 5 and 2 and 4, respectively. Cells were incubated at 37 °C with 5% CO_2 and plated at 0.4×10^5 cells/cm^2. The medium was changed every 2 days as well as 1 day prior to initiating experiments. The experiments started 4 days and 1 day post-confluence of the ARPE-19 and hf-RPE cells, respectively. tBH (Tokyo Kasei Kogyo Co., Ltd., Tokyo, Japan) was used to confer oxidative stress at the described concentrations and durations. The following cell death inhibitors were used: pan-caspase inhibitor Z-VAD-FMK (Z-VAD; AdipoGen, San Diego, CA, USA) at 50 μM, caspase 8 inhibitor (Ac-IETD; Sigma-Aldrich) at 50 μM, caspase 3 inhibitor (Ac-DEVD; Santa Cruz Biotechnology, Dallas, TX, USA) at 50 μM, receptor interacting protein 1 (RIP1) kinase inhibitors Necrostatin-1 (Nec-1; Santa Cruz Biotechnology) and Nec-1s (BioVision Inc., Milpitas, CA, USA) at 50 μM, lipid ROS scavenger ferrostatin-1 (Fer-1; Sigma-Aldrich) at 50 μM, and iron chelator deferoxamine mesylate (DFO; Santa Cruz) at 25 μM. Dimethyl sulfoxide (DMSO; Wako) was used as the vehicle as well as the control for inhibitor treatments at 0.16% in the medium. Treatment with these cell death inhibitors started 3 h prior to tBH exposure and continued until the end of the experiments. For the iron overload experiments, ARPE-19 cells were treated with ferric ammonium citrate (FAC; Wako) at the described concentrations for 2 days until the start of cell death inhibitor

treatment and/or tBH exposure (i.e., from day 2 to day 4 after confluence of the ARPE-19 cells).

2.2. Dehydrogenase activity and lactate dehydrogenase (LDH) leakage

ARPE-19 and hf-RPE cells seeded into 96-well plates were used. Dehydrogenase activity, which reflects cell viability, was assessed with the Cell Counting Kit-8 (CCK-8; Dojindo, Kumamoto, Japan) and a plate reader (2030 ARVO X3; Perkin Elmer, Waltham, MA, USA) for absorption measurements at 450 nm, according to the manufacturer's protocol. LDH leakage into the medium, which reflects cell membrane damage, was assessed with the Cytotoxicity LDH Assay Kit (Dojindo) and a plate reader for absorption measurements at 490 nm, according to the manufacturer's protocol.

2.3. Annexin V/propidium iodide (PI) staining

ARPE-19 cells seeded into chamber slides (8-well chamber slide II; AGC Techno Glass, Shizuoka, Japan) were used. After exposure to tBH, cells were washed with PBS and labeled with Annexin V and PI using the Annexin-V-FLUOS Staining Kit (Roche, Basel, Switzerland) according to manufacturer's protocol. Nuclei were stained with Hoechst 33342 (Thermo Fisher Scientific). After washing, the cells were observed under a fluorescence microscope (EX51; Olympus, Tokyo, Japan). For evaluation, we counted 800 cells per well and the number of apoptotic (Annexin V(+)/PI(−) for early apoptosis and Annexin V (+)/PI(+) for late apoptosis) and necrotic (Annexin V(−)/PI(+)) cells, and the findings were confirmed in triplicates.

2.4. Intracellular ROS, lipid peroxidation, and Fe^{2+}

ARPE-19 cells seeded into chamber slides and 96-well plates were used for assays. Intracellular ROS were assessed using treatment with 5 μM 5-(and-6)-chloromethyl-2′,7′-dichlorodihydrofluorescein diacetate, acetyl ester (CM-H2DCFDA; Thermo Fisher Scientific) in phenol red-free DMEM/F-12 medium. After washing, cells were observed under a fluorescence microscope (BZ-9000; Keyence, Osaka, Japan) or measured using a plate reader with filters for excitation around 488 nm and emission around 525 nm. Lipid peroxidation was assessed using treatment with 10 μM Bodipy 581/591C11 (Thermo Fisher Scientific) in phenol red-free DMEM/F-12 medium. After washing, cells were observed under a fluorescence microscope (BZ-9000, Keyence). Oxidized Bodipy and reduced Bodipy were observed using filters for green and red, respectively. Intracellular Fe^{2+} was assessed using treatment with 5 μM FeRhoNox-1 (Goryo Chemical, Inc., Sapporo, Japan) in Hank's balanced salt solution (HBSS; Thermo Fisher Scientific). After washing, the cells were observed under a fluorescence microscope (BZ-9000; Keyence). At least four fields per chamber were imaged, and the fluorescence intensities were analyzed with the Image-J system (https://imagej.nih.gov/ij/; provided in the public domain by the National Institutes of Health, Bethesda, MD, USA). The fluorescence intensities were corrected by the number of cells in the same field.

2.5. Intracellular glutathione (GSH)

ARPE-19 cells seeded into 6-well plates were used. Cells were harvested by scraping with 60 μL distilled water (DW), followed by sonication at 0 °C for 20 min and centrifugation at 15,000 × *g* at 4 °C for 10 min. The cell-free supernatant was used for analyzing total protein concentration with the Pierce BCA Protein Assay Kit (BCA assay; Thermo Fisher Scientific), and for analyzing GSH levels with the GSSG/GSH Quantification Kit (GSH assay; Dojindo). To remove protein from the samples prior to the GSH assay, 1/5 volume of 5% 5-sulfosalicylic acid dihydrate (SSA; Wako) in DW was added. After sample centrifugation at 15000 × *g* at 4 °C for 10 min, the supernatant was applied to the GSH assay. The protein and GSH concentrations of the samples were measured according to the manufacturers' protocols using a plate reader to measure absorbance at 405 nm. Values for the GSH levels were corrected by the protein concentration in the same sample.

2.6. Real-time RT-PCR

ARPE-19 cells seeded into 24-well plates were used. RNA was extracted with the TRI Reagent (Cosmo Bio, Carlsbad, CA, USA) according to the manufacturer's instructions. RNA pellets were resuspended in 10 μL RNase-free water and RNA was quantified with a NanoDrop 2000 spectrophotometer (Thermo Fisher Scientific). RNA was reverse-transcribed to cDNA with the ReverTra Ace qPCR RT Master Mix with gDNA Remover (Toyobo Co., Ltd, Osaka, Japan) according to manufacturer's protocol. SYBR Premix Ex Taq (Takara Bio Inc., Shiga, Japan) was used for real-time RT-PCR on the Thermal Cycler Dice Real System II TP900 (Takara Bio Inc.). The primer sequences are listed in Supplementary Table 1. Relative gene expression was calculated with the standard curve method, and the amount of each target mRNA was corrected by the expression level of the housekeeping gene, GAPDH, prior to gene comparisons. All reactions were performed in technical triplicates (three real-time RT-PCR replicates per well).

2.7. Statistical analyses

Data are presented as the mean ± standard error of the mean (SEM). All statistical analyses were performed using the GraphPad Prism program (GraphPad Software Inc., San Diego, CA). Values with $p < 0.05$ were considered statistically significant.

3. Results

3.1. Ferroptosis inhibitors rescue RPE cell death induced by oxidative stress

We first confirmed that the dehydrogenase activity assay and LDH leakage assay had similar sensitivities toward detecting decreased viability of ARPE-19 cells, by exposing these cells to different concentrations (0–600 μM) of tBH for 18 h (Supplementary Fig. 1A), or at a tBH concentration of 500 μM for different durations (Supplementary Fig. 1B). We next tested the effects of inhibitors toward apoptosis, necroptosis, and ferroptosis on cell viability while the cells were simultaneously exposed to 500 μM tBH for 18 h. We observed that the caspase inhibitors (Ac-DEVD, Ac-IETD, and Z-VAD), necroptosis inhibitors (Nec-1 and Nec-1s), and ferroptosis inhibitors (Fer-1 and DFO), were all able to rescue cell viability in the presence of lower tBH concentrations (Fig. 1A and B). However, at higher concentrations of

tBH, only the ferroptosis inhibitors were able to rescue the cell viability of the ARPE-19 cells (Fig. 1A–B). Similarly, for primary hf-RPE cells, ferroptosis inhibitors were more effective in rescuing cell viability than apoptosis or necroptosis inhibitors at both lower and higher concentrations of tBH (Supplementary Fig. 1C).

Recently a study has indicated that Fer-1 may not be a specific inhibitor of lipoxygenases (LOXs) (Zilka et al., 2017). Therefore, we further confirmed the ferroptotic ARPE-19 cell death under oxidative stress through observation that a 5-LOX inhibitor zileuton ameliorate tBH-induced cell death (Supplementary Fig. 2A). In addition, we observed that RSL3, an inhibitor of glutathione peroxidase 4 (GPx4), effectively induces cell death in ARPE-19 cells (Supplementary Fig. 2B). Since GPx4 is the dominant regulator of ferroptotic pathway (Cao and Dixon, 2016; Dixon et al., 2012), the results confirmed the susceptibility of ARPE-19 cells to ferroptosis.

3.2. Annexin-V/PI staining after tBH exposure

Because inhibitors of different modes of cell death were observed to ameliorate the decreased cell viability caused by tBH-mediated oxidative stress, we next assessed whether both apoptotic cells and necrotic cells were present under oxidative stress by staining the cells with Annexin V/PI during treatment with 500 μM tBH (Fig. 2). We observed that after 2–4 h of tBH exposure, the major staining pattern was Annexin V(+)/PI(−), indicating apoptosis. After 4–6 h, the number of cells with Annexin V(−)/PI(+) staining dramatically increased, whereas the number of apoptotic cells (Annexin V(+) with or without PI(+)) did not change significantly (Fig. 2), suggesting that both apoptotic and necrotic ARPE-19 cells exist under oxidative stress. In addition, ferroptosis inhibitors (Fer-1 and DFO) drastically decreased the number of PI(+) only necrotic cells, while apoptotic cells were retained (Supplementary Fig. 3).

3.3. Lipid peroxidation and GSH depletion after tBH exposure

Lipid peroxidation and GSH depletion are major hallmarks of ferroptotic cell death (Bertrand, 2017; Cao and Dixon, 2016; Dixon et al., 2012). We first assessed the intracellular levels of total ROS and lipid peroxidation in ARPE-19 cells exposed to 500 μM tBH (Fig. 3). Total ROS levels as depicted with the CM-H2DCFDA probe were upregulated at 3 and 6 h, but this upregulation was significantly suppressed by Fer-1 and DFO treatment (Fig. 3A). Upregulated lipid peroxidation as assessed with Bodipy was also evident after 1 and 3 h of tBH exposure (Fig. 3B), and this upregulation was also significantly suppressed by Fer-1 and DFO treatment (Fig. 3C).

Intracellular GSH levels were significantly downregulated in ARPE-19 cells exposed to either non-lethal (150 μM) or lethal (500 μM) tBH concentrations for up to 3 h (Fig. 4A). The depleted GSH levels were replenished up to more than baseline levels in cells under non-lethal tBH conditions, whereas the GSH levels remained depleted in cells under lethal tBH conditions (Fig. 4A). When treated with Fer-1 or DFO while exposed to the lethal tBH concentration of 500 μM, GSH depletion was significantly attenuated (Fig. 4B).

3.4. Intracellular Fe^{2+} levels and Fe^{2+} overload

Another hallmark of ferroptosis is iron dependency (Bertrand, 2017; Cao and Dixon, 2016; Dixon et al., 2012). Although we had already shown that the iron chelator DFO rescues tBH-induced cell death (Fig. 1), we further investigated this dependency by measuring intracellular Fe^{2+} levels with FeRhoNox-1 in ARPE-19 cells after exposure to 500 μM tBH. As shown in Fig. 5A, increased intracellular Fe^{2+} was observed after tBH exposure, and this was abrogated by Fer-1 and DFO treatment. Next, we examined the effect of iron overload on tBH-induced cell death using FAC pretreatment of the cells over 2 days prior to tBH exposure. When the cells were exposed to the non-lethal tBH concentration of 200 μM, FAC pretreatment dose-dependently decreased cell viability as assessed by decreased dehydrogenase activity (Fig. 5B), increased LDH leakage (Fig. 5C), and markedly increased intracellular Fe^{2+} levels (Fig. 5D). In addition, we observed that 120 μM FAC pretreatment for 2 days sensitized ARPE-19 cells to cell death induced by tBH exposure, but this was significantly attenuated by treatment with Fer-1 and DFO (Fig. 5E–F).

3.5. Effect of oxidative stress on the expression of iron homeostasis-regulating genes

To clarify the effects of oxidative stress on intracellular iron homeostasis, we evaluated the effect of 500 μM tBH exposure on the mRNA levels of genes involved in iron uptake, intracellular iron metabolism and trafficking, and iron release from ARPE-19 cells (Fig. 6). The mRNA levels of the transferrin receptor 1 (TFRC) that mediates iron import were significantly upregulated by tBH exposure. The mRNA levels of six-transmembrane epithelial antigen of prostate 3 (STEAP3) and divalent metal transporter 1 (DMT1), which facilitate ferrous iron transport to the cytoplasm, were significantly downregulated. The mRNA levels of IREB1 and IREB2, master regulators of iron metabolism, were significantly downregulated by tBH. Ferritin L (FTL) and H (FTH) subunits transport ferrous iron in the cytoplasm to lysosome for storage. In our experiment, mRNA levels of FTL were significantly upregulated, while those of FTH were insignificantly upregulated by tBH. The mRNA levels of hephaestin (HEPH) and ferroportin 1 (FPN1), which participate in oxidizing excessive ferrous iron into ferric iron for export, were downregulated.

4. Discussion

Since several lines of evidence support the hypothesis that RPE cell death is induced by oxidative stress and that elevated iron levels in RPE are implicated in AMD pathogenesis (Chen et al., 2009; Hahn et al., 2003, 2006; Junemann et al., 2013), we investigated the modes of oxidative stress-induced cell death in RPE cells *in vitro*. We found that both apoptotic and necrotic cells exist under lethal oxidative stress. Notably, ferroptotic inhibitors were more effective than inhibitors of apoptosis or necroptosis in rescuing cell death in both ARPE-19 cells and primary RPE cells.

Previous studies have described the apoptotic features of RPE cell death induced by H_2O_2 or tBH based on the following characteristics: caspase 3 activation (detected directly (Sreekumar et al., 2013; Sreekumar et al., 2005) or indirectly (Alge et al., 2002; Cai et al., 1999; Jeung et al., 2016; Rodrigues et al., 2011)), Annexin V positivity (Barak et al., 2001; Cai et al., 1999; Jeung et al., 2016; Rodrigues et al., 2011), release of cytochrome *c* into the

cytosol (Cai et al., 1999), non-randomized DNA fragmentation (Eichler et al., 2008), and increased cell viability by Bcl-2 overexpression (Godley et al., 2002). However, some studies have shown not only apoptosis but also necrosis detection with Annexin V/PI staining (Barak et al., 2001; Jeung et al., 2016; Kim et al., 2003), which is consistent with our results. On the other hand, a recent study suggested necroptosis to be the major mechanism of ARPE-19 cell death induced by H_2O_2 or tBH, based on observations including the aggregation of receptor interacting protein kinase 3 (RIPK3), cell death amelioration by Nec-1 or RIPK3 silencing, nuclear and plasma membrane leakage and breakdown, absence of cleaved caspase 3 or DNA fragmentation, and lack of cell death inhibition by Z-VAD (Hanus et al., 2013). This ineffectiveness reported for Z-VAD is contradictory to the results of our study and those of many other studies; however, this inconsistency may have arisen because of differences in cell confluency and pretreatment duration with Z-VAD between studies (subconfluency and 24 h, respectively (Hanus et al., 2013)). Our results indicate that not only apoptosis but also regulated necrosis, including necroptosis and ferroptosis, occur in RPE cells under oxidative stress.

Ferroptosis is characterized by (i) GSH depletion and lipid peroxidation, (ii) iron-dependent intracellular ROS accumulation and acceleration of cell death with iron overload, and (iii) rescue by lipid ROS scavengers such as Fer-1 and iron chelators such as DFO (Bertrand, 2017; Cao and Dixon, 2016; Dixon et al., 2012). In our study, we observed GSH depletion and the accumulation of peroxidized lipids under oxidative stress, which were both attenuated by Fer-1 and DFO. In addition, iron overload increased intracellular Fe^{2+} and made ARPE-19 cells susceptible to lower concentrations of tBH, which was also ameliorated by Fer-1 and DFO. Therefore, our observations further support iron-dependent ferroptotic cell death of RPE cells under oxidative stress.

A recently publicshed study (Sun et al., 2018) has shown that GSH depletion, a ferroptotic stimulus, induces ferroptosis, autophagy and premature senescence in ARPE-19 cells. The same study further suggested the involvement of autophagy in the process of ferroptosis and premature senescence induced by GSH depletion.

In literature several ultrastructual changes have been reported for ferroptotic cell death. In BJeLR cells mitochondrial shrinkage and reduced cristae have been observed, while in kidney tissue mitochondrial rupture has been reported (Xie et al., 2016). In ferroptotic ARPE-19 cells, increased number of autophagosomes has been reported (Sun et al., 2018). Therefore, further investigations are necessary to address the ferroptosis-specific ultrastructual changes.

Intracellular Fe^{2+} levels have been shown to increase during the ferroptosis of other cell types (Aron et al., 2016), which is consistent with our results where the increase in intracellular Fe^{2+} levels in ARPE-19 cells under oxidative stress was abolished by Fer-1, a lipid ROS scavenger and ferroptosis inhibitor. Furthermore, in the present study, we assessed changes in the mRNA expression to understand how oxidative stress influences regulators of intracellular Fe^{2+}. We observed downregulation of STEAP3, DMT1, IREB1, and IREB2 and upregulation of FTL mRNA levels after tBH exposure. These changes are considered to suppress intracellular Fe^{2+} levels, suggesting a compensatory response to increased Fe^{2+}. In

contrast, the mRNA level of TFRC was upregulated, whereas the levels of FPN1 and HEPH were downregulated after tBH exposure. As these changes are considered to increase cytosolic Fe^{2+} levels, these iron homeostasis regulators may have causative roles in oxidative stress-induced ferroptotic RPE cell death.

The underlying mechanisms of increased intracellular Fe^{2+} under oxidative stress are still unknown. Previous studies have reported that oxidative stress promotes iron uptake via IREB1 activation-mediated TFRC upregulation in B6 fibroblasts (Andriopoulos et al., 2007) and rat liver (Mueller et al., 2001), and that IREB1 activation mediates a positive feedback loop between oxidative stress and increased iron uptake in neuroblastoma (N2a) cells (Núñez-Millacura et al., 2002), and oxidative stress may also induce degradation of ferroportin proteins in neuroblastoma (SH-SY5Y) cells (Dev et al., 2015). Our observations of downregulated FPN1 and HEPH and upregulated TFRC mRNA levels may hint at the mechanisms underlying increased iron levels in RPE cells under oxidative stress, but further investigations are required.

In ferroptosis, three processes, (i) accumulation of Fe^{2+}, (ii) glutathione depletion, and (iii) lipid peroxidation, are considered to unfold simultaneously, and these three events amplify each other through positive feedback loops until some of these events exceed the cellular compensative ability (Bertrand, 2017). We confirmed these events in RPE cells under oxidative stress and observed that ferroptotic cell death could be disrupted by lipid ROS scavengers or iron chelators.

Ferroptotic cell death under oxidative stress insights the AMD pathogenesis, however, the observations *in vitro* using an acute stress model in undifferentiated ARPE-19 cells may not be relevant to the complex human AMD pathogenesis. In our study, Fer-1 and DFO worked similarly to prevent ARPE-19 cell death while Fer-1 worked better than DFO in primary human RPE cells, indicating these two axes of tBH-induced cell death are not synonymous. Detail on the RPE ferroptosis under oxidative stress need to be further addressed.

In conclusion, we suggest that RPE cell death induced by oxidative stress may include ferroptosis in addition to apoptosis and necroptosis. Lipid peroxidation and intracellular iron levels may, therefore, prove suitable candidates as therapeutic targets for dry AMD.

Supplementary Material

Refer to Web version on PubMed Central for supplementary material.

Acknowledgement

This work was supported by Japan Society of Promotion of Science (26861437), Nakayama Foundation for Human Science (H26), and Mitsui Sumitomo Insurance Welfare Foundation (H26).

References

Adler R, Curcio C, Hicks D, Price D, Wong F, 1999 Cell death in age-related macular degeneration. Mol. Vis 5, 31. [PubMed: 10562655]

Age-Related Eye Disease Study Research Group, 2001 A randomized, placebo-controlled, clinical trial of high-dose supplementation with vitamins C and E, beta carotene, and zinc for age-related macular degeneration and vision loss. Arch. Ophthalmol 119, 1417–1436. [PubMed: 11594942]

Alge CS, Priglinger SG, Neubauer AS, Kampik A, Zillig M, Bloemendal H, Welge-Lussen U, 2002 Retinal pigment epithelium is protected against apoptosis by alphaB-crystallin. Invest. Ophthalmol. Vis. Sci 43, 3575–3582. [PubMed: 12407170]

Andriopoulos B, Hegedusch S, Mangin J, Riedel HD, Hebling U, Wang J,Pantopoulos K, Mueller S, 2007 Sustained hydrogen peroxide induces iron uptake by transferrin receptor-1 independent of the iron regulatory protein/iron-responsive element network. J. Biol. Chem 282, 20301–20308. [PubMed: 17517884]

Aron AT, Loehr MO, Bogena J, Chang CJ, 2016 An endoperoxide reactivity-based FRET probe for ratiometric fluorescence imaging of labile iron pools in living cells. J. Am. Chem. Soc 138, 14338–14346. [PubMed: 27768321]

Barak A, Morse LS, Goldkorn T, 2001 Ceramide: a potential mediator of apoptosis in human retinal pigment epithelial cells. Invest. Ophthalmol. Vis. Sci 42, 247–254. [PubMed: 11133876]

Beatty S, Koh H, Phil M, Henson D, Boulton M, 2000 The role of oxidative stress in the pathogenesis of age-related macular degeneration. Surv. Ophthalmol 45, 115–134. [PubMed: 11033038]

Bertrand RL, 2017 Iron accumulation, glutathione depletion, and lipid peroxidation must occur simultaneously during ferroptosis and are mutually amplifying events. Med. Hypotheses 101, 69–74. [PubMed: 28351498]

Bressler NM, Munoz B, Maguire MG, Vitale SE, Schein OD, Taylor HR, West SK, 1995 Five-year incidence and disappearance of drusen and retinal pigment epithelial abnormalities. Waterman study. Arch. Ophthalmol 113, 301–308. [PubMed: 7534060]

Cai J, Wu M, Nelson KC, Sternberg P Jr., Jones DP, 1999 Oxidant-induced apoptosis in cultured human retinal pigment epithelial cells. Invest. Ophthalmol. Vis. Sci 40, 959–966. [PubMed: 10102293]

Cao JY, Dixon SJ, 2016 Mechanisms of ferroptosis. Cell. Mol. Life Sci 73, 2195–2209. [PubMed: 27048822]

Chen H, Lukas TJ, Du N, Suyeoka G, Neufeld AH, 2009 Dysfunction of the retinal pigment epithelium with age: increased iron decreases phagocytosis and lysosomal activity. Invest. Ophthalmol. Vis. Sci 50, 1895–1902. [PubMed: 19151392]

Chou R, Dana T, Bougatsos C, Grusing S, Blazina I, 2016 Screening for impaired visual acuity in older adults: updated evidence report and systematic review for the US preventive services task force. J. Am. Med. Assoc 315, 915–933.

Curcio CA, Zanzottera EC, Ach T, Balaratnasingam C, Freund KB, 2017 Activated retinal pigment epithelium, an optical coherence tomography biomarker for progression in age-related macular degeneration. Invest. Ophthalmol. Vis. Sci 58, BIO211–BIO226. [PubMed: 28785769]

Dev S, Kumari S, Singh N, Kumar Bal S, Seth P, Mukhopadhyay CK, 2015 Role of extracellular Hydrogen peroxide in regulation of iron homeostasis genes in neuronal cells: implication in iron accumulation. Free Radic. Biol. Med 86, 78–89. [PubMed: 26006106]

Dixon SJ, Lemberg KM, Lamprecht MR, Skouta R, Zaitsev EM, Gleason CE, Patel DN, Bauer AJ, Cantley AM, Yang WS, Morrison B 3rd, Stockwell BR, 2012 Ferroptosis: an iron-dependent form of nonapoptotic cell death. Cell 149, 1060–1072. [PubMed: 22632970]

Do Van B, Gouel F, Jonneaux A, Timmerman K, Gele P, Petrault M, Bastide M, Laloux C, Moreau C, Bordet R, Devos D, Devedjian JC, 2016 Ferroptosis, a newly characterized form of cell death in Parkinson's disease that is regulated by PKC. Neurobiol. Dis 94, 169–178. [PubMed: 27189756]

Eichler W, Reiche A, Yafai Y, Lange J, Wiedemann P, 2008 Growth-related effects of oxidant-induced stress on cultured RPE and choroidal endothelial cells. Exp. Eye Res 87, 342–348. [PubMed: 18640112]

Evans JR, 2001 Risk factors for age-related macular degeneration. Prog. Retin. Eye Res20, 227–253. [PubMed: 11173253]

Friedmann Angeli JP, Schneider M, Proneth B, Tyurina YY, Tyurin VA, Hammond VJ, Herbach N, Aichler M, Walch A, Eggenhofer E, Basavarajappa D, Radmark O, Kobayashi S, Seibt T, Beck H, Neff F, Esposito I, Wanke R, Forster H, Yefremova O, Heinrichmeyer M, Bornkamm GW, Geissler

EK, Thomas SB, Stockwell BR, O'Donnell VB, Kagan VE, Schick JA, Conrad M, 2014 Inactivation of the ferroptosis regulator Gpx4 triggers acute renal failure in mice. Nat. Cell Biol 16, 1180–1191. [PubMed: 25402683]

Fritsche LG, Igl W, Bailey JN, Grassmann F, Sengupta S, Bragg-Gresham JL, Burdon KP, Hebbring SJ, Wen C, Gorski M, Kim IK, Cho D, Zack D, Souied E, Scholl HP, Bala E, Lee KE, Hunter DJ, Sardell RJ, Mitchell P, Merriam JE, Cipriani V, Hoffman JD, Schick T, Lechanteur YT, Guymer RH, Johnson MP, Jiang Y, Stanton CM, Buitendijk GH, Zhan X, Kwong AM, Boleda A, Brooks M, Gieser L, Ratnapriya R, Branham KE, Foerster JR, Heckenlively JR, Othman MI, Vote BJ, Liang HH, Souzeau E, McAllister IL, Isaacs T, Hall J, Lake S, Mackey DA, Constable IJ, Craig JE, Kitchner TE, Yang Z, Su Z, Luo H, Chen D, Ouyang H, Flagg K, Lin D, Mao G, Ferreyra H, Stark K, von Strachwitz CN, Wolf A, Brandl C, Rudolph G, Olden M, Morrison MA, Morgan DJ, Schu M, Ahn J, Silvestri G, Tsironi EE, Park KH, Farrer LA, Orlin A, Brucker A, Li M, Curcio CA, Mohand-Said S, Sahel JA, Audo I, Benchaboune M, Cree AJ, Rennie CA, Goverdhan SV, Grunin M, Hagbi-Levi S, Campochiaro P, Katsanis N, Holz FG, Blond F, Blanche H, Deleuze JF, Igo RP Jr., Truitt B, Peachey NS, Meuer SM, Myers CE, Moore EL, Klein R, Hauser MA, Postel EA, Courtenay MD, Schwartz SG, Kovach JL, Scott WK, Liew G, Tan AG, Gopinath B, Merriam JC, Smith RT, Khan JC, Shahid H, Moore AT, McGrath JA, Laux R, Brantley MA Jr., Agarwal A, Ersoy L, Caramoy A, Langmann T, Saksens NT, de Jong EK, Hoyng CB, Cain MS, Richardson AJ, Martin TM, Blangero J, Weeks DE, Dhillon B, van Duijn CM, Doheny KF, Romm J, Klaver CC, Hayward C, Gorin MB, Klein ML, Baird PN, den Hollander AI, Fauser S, Yates JR, Allikmets R, Wang JJ, Schaumberg DA, Klein BE, Hagstrom SA, Chowers I, Lotery AJ, Leveillard T, Zhang K, Brilliant MH, Hewitt AW, Swaroop A, Chew EY, Pericak-Vance MA, DeAngelis M, Stambolian D, Haines JL, Iyengar SK, Weber BH, Abecasis GR, Heid IM, 2016 A large genome-wide association study of age-related macular degeneration highlights contributions of rare and common variants. Nat. Genet 48, 134–143. [PubMed: 26691988]

Godley BF, Jin G-F, Guo Y-S, Hurst JS, 2002 Bcl-2 overexpression increases survival in human retinal pigment epithelial cells exposed to H2O2. Exp. Eye Res 74, 663–669. [PubMed: 12126940]

Hahn P, Milam AH, Dunaief JL, 2003 Maculas affected by age-related macular degeneration contain increased chelatable iron in the retinal pigment epithelium and Bruch's membrane. Arch. Ophthalmol 121, 1099–1105. [PubMed: 12912686]

Hahn P, Ying GS, Beard J, Dunaief JL, 2006 Iron levels in human retina: sex difference and increase with age. Neuroreport 17, 1803–1806. [PubMed: 17164668]

Halliwell B, Gutteridge JMC, 1984 Oxygen toxicity, oxygen radicals, transition metals and disease. Biochem. J 219, 1–14. [PubMed: 6326753]

Hanus J, Zhang H, Wang Z, Liu Q, Zhou Q, Wang S, 2013 Induction of necrotic cell death by oxidative stress in retinal pigment epithelial cells. Cell Death Dis. 4, e965. [PubMed: 24336085]

Hanus J, Anderson C, Sarraf D, Ma J, Wang S, 2016 Retinal pigment epithelial cell necroptosis in response to sodium iodate. Cell Death Dis. 2, 16054.

Jeung IC, Jee D, Rho CR, Kang S, 2016 Melissa officinalis L. Extracts protect human retinal pigment epithelial cells against oxidative stress-induced apoptosis. Int.J. Med. Sci 13, 139–146.

Junemann AG, Stopa P, Michalke B, Chaudhri A, Reulbach U, Huchzermeyer C, Schlotzer-Schrehardt U, Kruse FE, Zrenner E, Rejdak R, 2013 Levels of aqueous humor trace elements in patients with non-exsudative age-related macular degeneration: a case-control study. PLoS One 8, e56734. [PubMed: 23457607]

Kaarniranta K, Ryhanen T, Karjalainen HM, Lammi MJ, Suuronen T, Huhtala A, Kontkanen M, Terasvirta M, Uusitalo H, Salminen A, 2005 Geldanamycin increases 4-hydroxynonenal (HNE)-induced cell death in human retinal pigment epithelial cells. Neurosci. Lett 382, 185–190. [PubMed: 15911146]

Kim MH, Chung J, Yang JW, Chung SM, Kwag NH, Yoo JS, 2003 Hydrogen peroxide-induced cell death in a human retinal pigment epithelial cell line, ARPE-19. Kor. J. Ophthalmol 17, 19–28.

Kim JH, Kim JH, Jun HO, Yu YS, Min BH, Park KH, Kim KW, 2010 Protective effect of clusterin from oxidative stress-induced apoptosis in human retinal pigment epithelial cells. Invest. Ophthalmol. Vis. Sci 51, 561–566. [PubMed: 19710412]

Li GY, Fan B, Zheng YC, 2010 Calcium overload is a critical step in programmed necrosis of ARPE-19 cells induced by high-concentration H2O2. Biomed. Environ. Sci 23, 371–377. [PubMed: 21112485]

Miller JW, 2010 Treatment of age-related macular degeneration: beyond VEGF. Jpn. J.Ophthalmol 54, 523–528. [PubMed: 21191711]

Miller JW, 2013 Age-related macular degeneration revisited–piecing the puzzle: the LXIX Edward Jackson memorial lecture. Am. J. Ophthalmol 155, 1–35 e13. [PubMed: 23245386]

Miller JW, 2016 VEGF: from discovery to therapy: the champalimaud award lecture. Transl Vis Sci Technol 5, 9.

Miller JW, Bagheri S, Vavvas DG, 2017 Advances in age-related macular degeneration understanding and therapy. US Ophthalmic Rev 10, 119–130. [PubMed: 29142592]

Moreno-Gonzalez G, Vandenabeele P, Krysko DV, 2016 Necroptosis: a novel cell death modality and its potential relevance for critical care medicine. Am. J. Respir. Crit. Care Med 194, 415–428. [PubMed: 27285640]

Mueller S, Pantopoulos K, Hubner CA, Stremmel W, Hentze MW, 2001 IRP1 activation by extracellular oxidative stress in the perfused rat liver. J. Biol. Chem 276, 23192–23196. [PubMed: 11297549]

Murakami Y, Matsumoto H, Roh M, Giani A, Kataoka K, Morizane Y, Kayama M, Thanos A, Nakatake S, Notomi S, Hisatomi T, Ikeda Y, Ishibashi T, Connor KM, Miller JW, Vavvas DG, 2014 Programmed necrosis, not apoptosis, is a key mediator of cell loss and DAMP-mediated inflammation in dsRNA-induced retinal degeneration. Cell Death Differ. 21, 270–277. [PubMed: 23954861]

Núñez-Millacura C, Tapia V, Muñoz P, Maccioni RB, Núñez MT, 2002 An oxidative stress-mediated positive-feedback iron uptake loop in neuronal cells. J. Neurochem 82, 240–248. [PubMed: 12124425]

Rodrigues GA, Maurier-Mahe F, Shurland DL, McLaughlin A, Luhrs K, Throo E, Delalonde-Delaunay L, Pallares D, Schweighoffer F, Donello J, 2011 Differential effects of PPARgamma ligands on oxidative stress-induced death of retinal pigmented epithelial cells. Invest. Ophthalmol. Vis. Sci 52, 890–903. [PubMed: 20847119]

Rosenfeld PJ, Schwartz SD, Blumenkranz MS, Miller JW, Haller JA, Reimann JD, Greene WL, Shams N, 2005 Maximum tolerated dose of a humanized anti-vascular endothelial growth factor antibody fragment for treating neovascular age-related macular degeneration. Ophthalmology 112, 1048–1053. [PubMed: 15885778]

Schmitz-Valckenberg S, Bindewald-Wittich A, Dolar-Szczasny J, Dreyhaupt J, Wolf S, Scholl HP, Holz FG, Fundus Autofluorescence in Age-Related Macular Degeneration Study Group, 2006 Correlation between the area of increased auto-fluorescence surrounding geographic atrophy and disease progression in patients with AMD. Invest. Ophthalmol. Vis. Sci 47, 2648–2654. [PubMed: 16723482]

Sharma A, Sharma R, Chaudhary P, Vatsyayan R, Pearce V, Jeyabal PV, Zimniak P, Awasthi S, Awasthi YC, 2008 4-Hydroxynonenal induces p53-mediated apoptosis in retinal pigment epithelial cells. Arch. Biochem. Biophys 480, 85–94. [PubMed: 18930016]

Shintoku R, Takigawa Y, Yamada K, Kubota C, Yoshimoto Y, Takeuchi T,Koshiishi I, Torii S, 2017 Lipoxygenase-mediated generation of lipid peroxides enhances ferroptosis induced by erastin and RSL3. Canc. Sci 108, 2187–2194.

Song D, Dunaief JL, 2013 Retinal iron homeostasis in health and disease. Front. Aging Neurosci 5, 24. [PubMed: 23825457]

Sreekumar PG, Kannan R, Yaung J, Spee CK, Ryan SJ, Hinton DR, 2005 Protection from oxidative stress by methionine sulfoxide reductases in RPE cells. Biochem. Biophys. Res. Commun 334, 245–253. [PubMed: 15993845]

Sreekumar PG, Chothe P, Sharma KK, Baid R, Kompella U, Spee C, Kannan N, Manh C, Ryan SJ, Ganapathy V, Kannan R, Hinton DR, 2013 Antiapoptotic properties of alpha-crystallin-derived peptide chaperones and characterization of their uptake transporters in human RPE cells. Invest. Ophthalmol. Vis. Sci 54, 2787–2798. [PubMed: 23532520]

Sun Y, Zheng Y, Wang C, Liu Y, 2018 Glutathione depletion induced ferroptosis, autophagy, and premature cell senescence in retinal pigment epithelial cells. Cell Death Dis. 9, 753. [PubMed: 29988039]

Suzuki M, Kamei M, Itabe H, Yoneda K, Bando H, Kume N, Tano Y, 2007 Oxidized phospholipids in the macula increase with age and in eyes with age-related macular degeneration. Mol. Vis 13, 772–778. [PubMed: 17563727]

Tate DJ Jr., Miceli MV, Newsome DA, 1995 Phagocytosis and H2O2 induce catalase and metallothionein gene expression in human retinal pigment epithelial cells. Invest. Ophthalmol. Vis. Sci 36, 9. [PubMed: 7822163]

Thornton J, Edwards R, Mitchell P, Harrison RA, Buchan I, Kelly SP, 2005 Smoking and age-related macular degeneration: a review of association. Eye 19, 935–944. [PubMed: 16151432]

Wang H, An P, Xie E, Wu Q, Fang X, Gao H, Zhang Z, Li Y, Wang X, Zhang J, Li G, Yang L, Liu W, Min J, Wang F, 2017 Characterization of ferroptosis in murine models of hemochromatosis. Hepatology 66, 449–465. [PubMed: 28195347]

Wong WL, Su X, Li X, Cheung CMG, Klein R, Cheng CY, Wong TY, 2014 Global prevalence of age-related macular degeneration and disease burden projection for 2020 and 2040: a systematic review and meta-analysis. The Lancet Global Health 2, e106–e116. [PubMed: 25104651]

Xie Y, Hou W, Song X, Yu Y, Huang J, Sun X, Kang R, Tang D, 2016 Ferroptosis: process and function. Cell Death Differ. 23, 369–379. [PubMed: 26794443]

Xu X, Liu X, Wang X, Clark ME, McGwin G Jr., Owsley C, Curcio CA, Zhang Y, 2017 Retinal pigment epithelium degeneration associated with subretinal drusenoid deposits in age-related macular degeneration. Am. J. Ophthalmol 175, 87–98. [PubMed: 27986424]

Yan T, Bi H, Wang Y, 2014 Wogonin modulates hydroperoxide-induced apoptosis via PI3K/Akt pathway in retinal pigment epithelium cells. Diagn. Pathol 9, 154. [PubMed: 25432585]

Zilka O, Shah R, Li B, Friedmann Angeli JP, Griesser M, Conrad M, Pratt DA, 2017 On the mechanism of cytoprotection by Ferrostatin-1 and Liproxstatin-1 and the role of lipid peroxidation in ferroptotic cell death. ACS Cent. Sci 3, 232–243. [PubMed: 28386601]

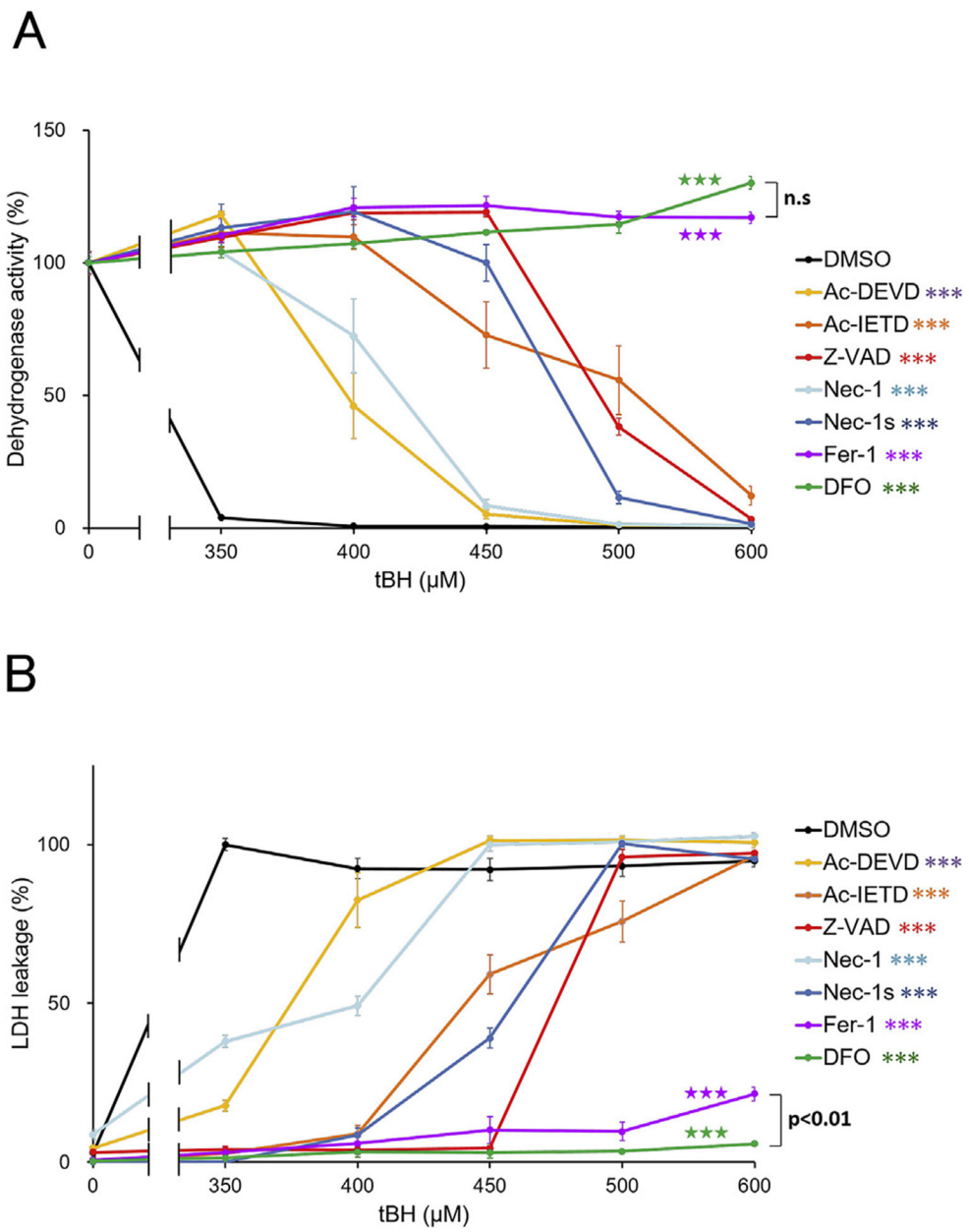

Fig. 1. Effects of cell death inhibitors on ARPE-19 cell viability under tBH exposure.

(**A, B**) Effects of cell death inhibitors on dehydrogenase activity (**A**) and LDH leakage (**B**) in ARPE-19 cells after exposure to tBH for 18 h. N = 5 per group. Significant differences (***$p < 0.001$) compared to DMSO vehicle group. Significant differences (★★★$p < 0.001$) compared to any other apoptosis/necroptosis inhibitors. No significant difference (ns) between Fer-1 and DFO treatments. Two-way ANOVA and post-hoc Tukey's test.

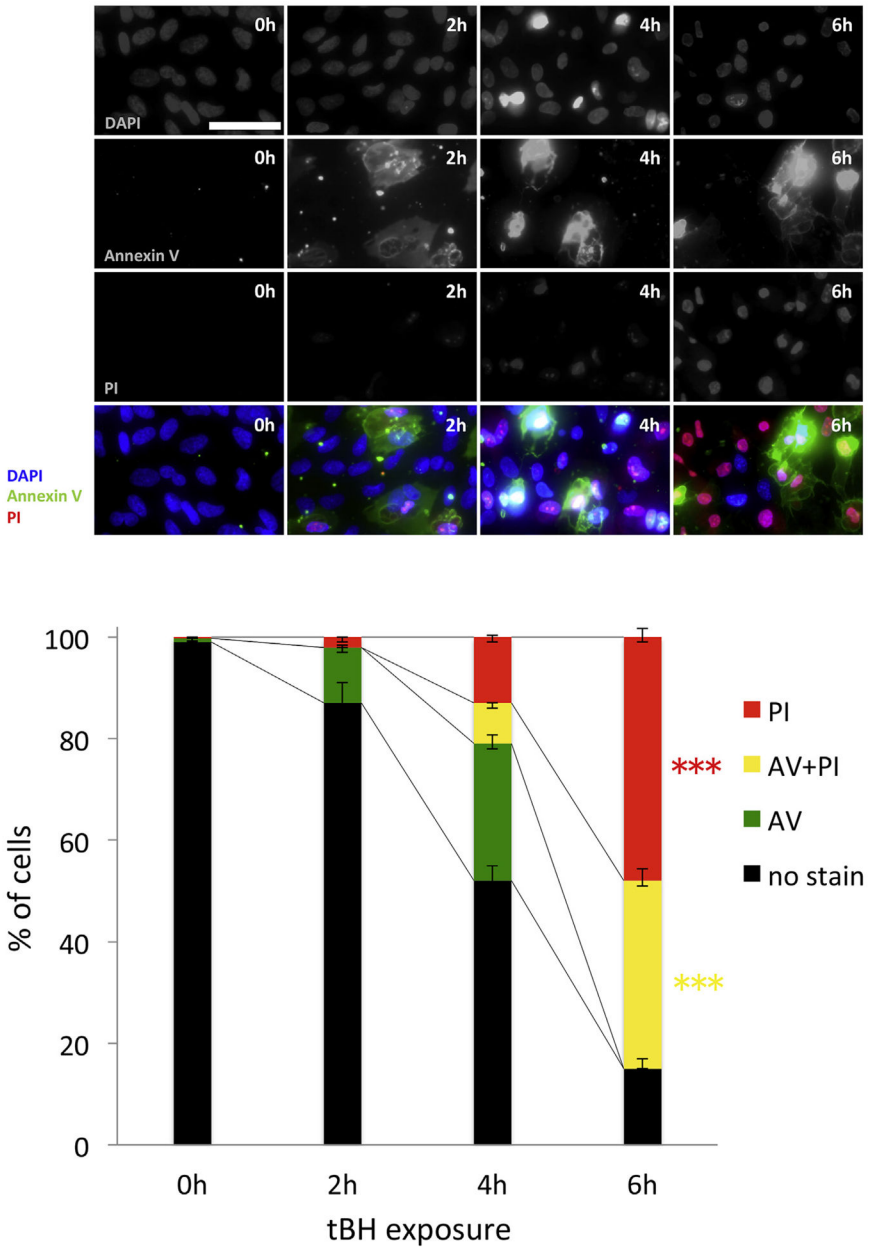

Fig. 2. Annexin V/PI staining of APRE-19 cells under tBH exposure.

Representative staining view at low and high magnifications at baseline (0 h) and with 500 μM tBH exposure for 2, 4, and 6 h. Scale bar, 50 μm. The graph shows the time course of the number of cells stained with Annexin V and PI after 500 μM tBH exposure. ***$p < 0.001$ by one-way ANOVA for the appearance of apoptotic and necrotic cells. N = 3 per group.

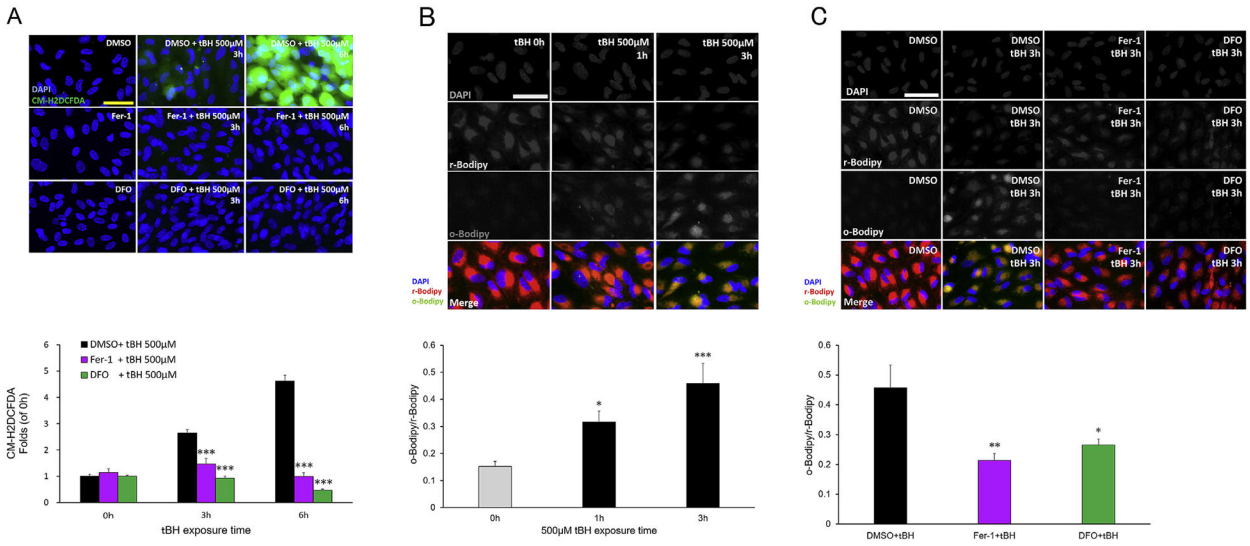

Fig. 3. Lipid peroxidation in ARPE-19 cells under 500 μM tBH exposure.

(**A**) Intracellular ROS was assessed using the CM-H2DCFDA probe at baseline (no tBH) and after 3 and 6 h of tBH exposure. The rescue effects of Fer-1 and DFO were also evaluated. Representative staining view. Scale bar, 50 μm. Quantification using a plate reader. N = 8 per group. ***$p < 0.001$ vs. DMSO vehicle only. One-way ANOVA and post-hoc Dunnett's test. (**B**) Intracellular lipid peroxidation was assessed using Bodipy 581/591C11 at baseline (no tBH) and after 1 and 3 h of tBH exposure. Representative staining view. Reduced (r-) and oxidized (o-) Bodipy. Scale bar, 50 μm. Staining intensity with *o*-Bodipy divided by the staining intensity with r-Bodipy was used to represent the extent of lipid peroxidation. N = 7–9 per group. *$p < 0.05$ and ***$p < 0.001$ vs. 0 h. Kruskal–Wallis and post-hoc Dunnett's test. (**C**) Representative view and quantification indicating rescue effects of Fer-1 and DFO after 3 h exposure to tBH. Scale bar, 50 μm. N = 6–9 per group. *$p < 0.05$ vs DMSO vehicle. One-way ANOVA and post-hoc Dunnett's test.

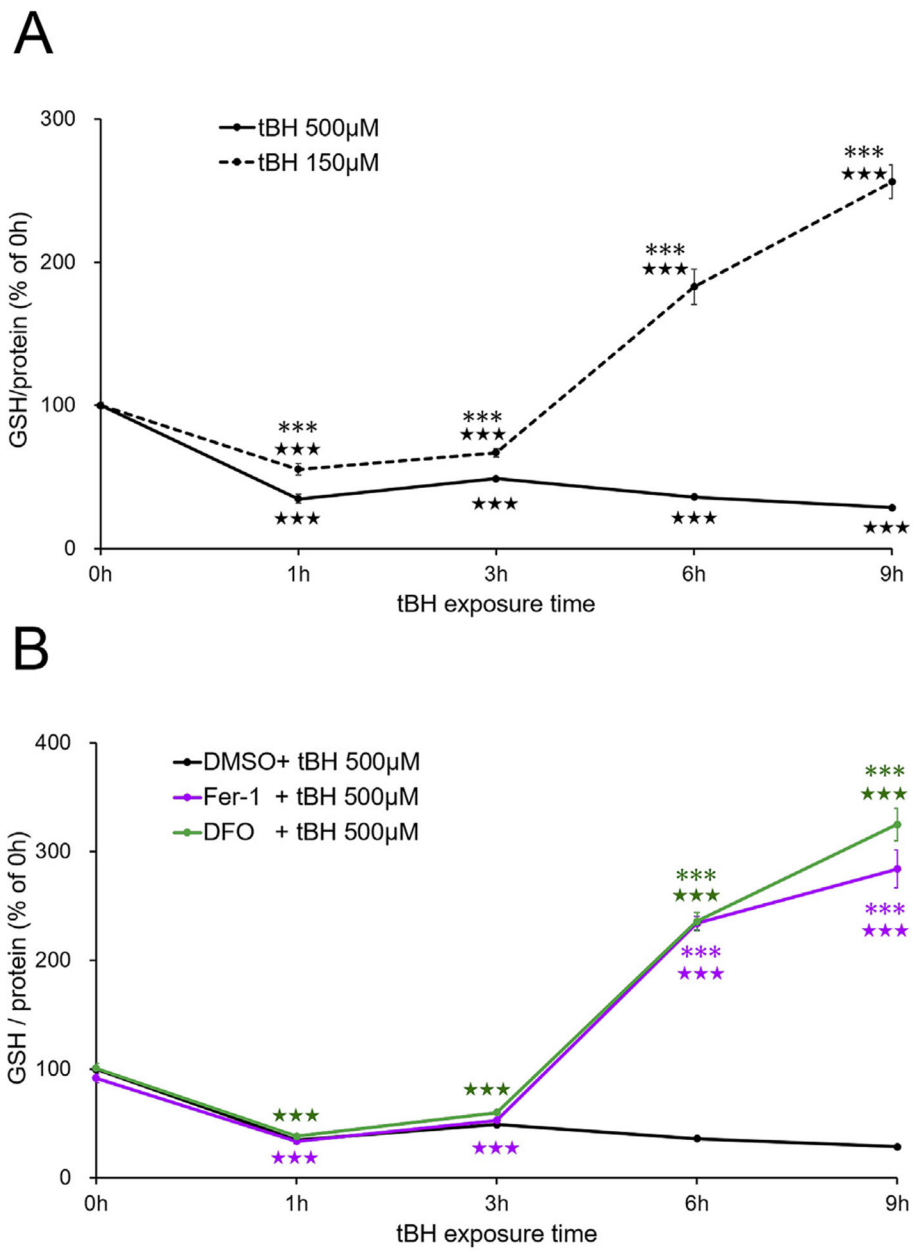

Fig. 4. Intracellular GSH levels in ARPE-19 cells under tBH exposure and rescue effects of Fer-1 and DFO.

(**A**) Degree of GSH depletion and replenishment under 150 and 500 μM tBH exposure. (**B**) Rescue effects of Fer-1 and DFO on GSH depletion under 500 μM tBH exposure. N = 6–12 per group. ***$p < 0.001$ vs. 500 μM tBH only. ★★★$p < 0.001$ vs. 0 h of the same group. One-way ANOVA and post-hoc Tukey's test.

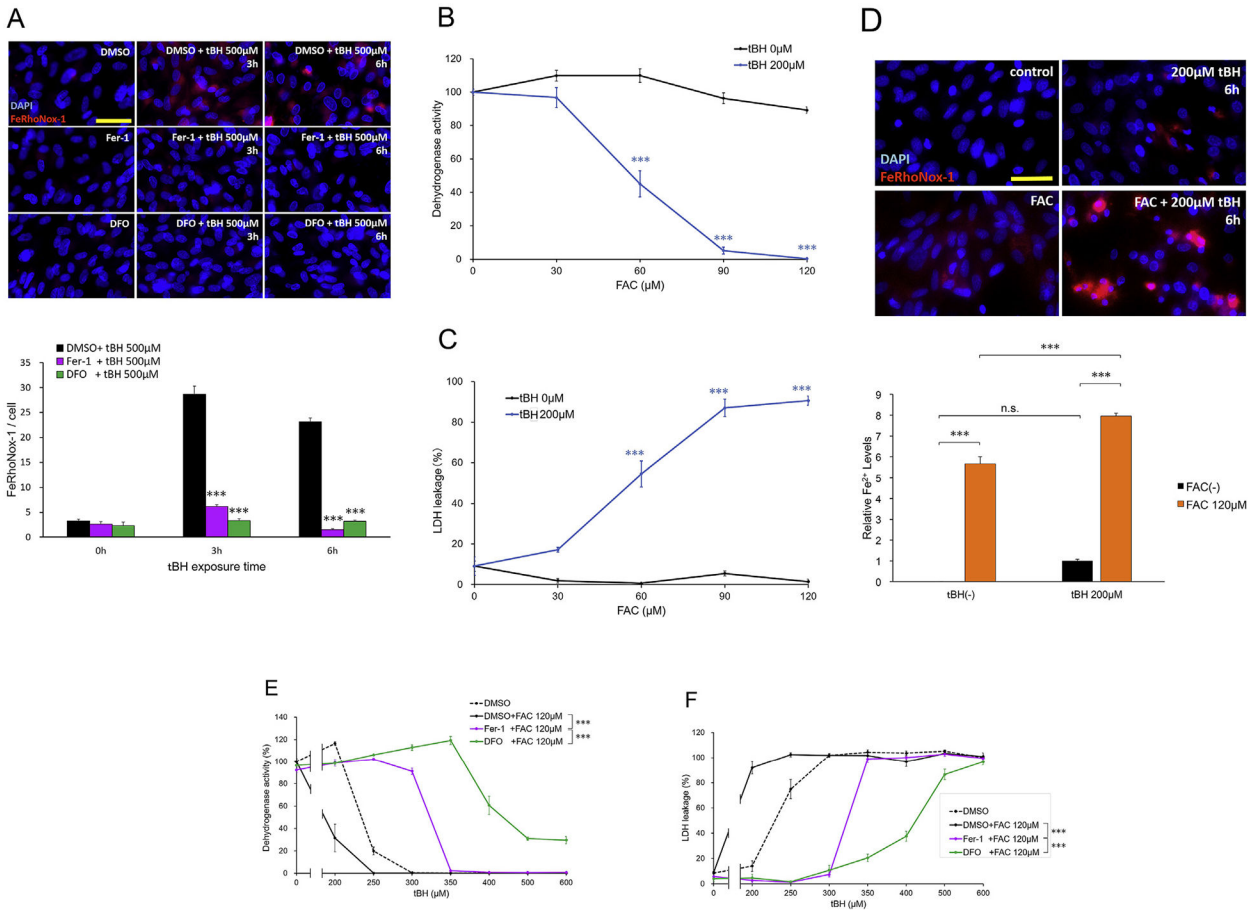

Fig. 5. Iron overload and susceptibility to ferroptotic cell death of ARPE-19 cells under tBH exposure.

(**A**) Intracellular Fe^{2+} levels under 500 μM tBH exposure and the effects of Fer-1 and DFO. Scale bar, 50 μm. N = 9–12 per group. ***p < 0.001 vs. 500 μM DMSO vehicle group only. One-way ANOVA and post-hoc Dunnett's test. (**B, C**) Dose-dependent effects of iron overload on dehydrogenase activity (**B**) and LDH leakage (**C**) under 0 or 200 μM tBH for 18 h. N = 5 per group. ***p < 0.001 vs. no FAC for the same group. One-way ANOVA and post-hoc Dunnett's test. (**D**) The effect of iron overload with or without 200 μM tBH exposure for 6 h on intracellular Fe^{2+} levels. N = 5 per group. ***p < 0.001; n.s., not significant; one-way ANOVA and post-hoc Tukey's test. (**E, F**) Rescue effects of Fer-1 and DFO on dehydrogenase activity (**E**) and LDH leakage (**F**) under iron overload (120 μM FAC) and tBH exposure for 18 h. N = 5 per group. ***p < 0.001, two-way ANOVA and post-hoc Tukey's test.

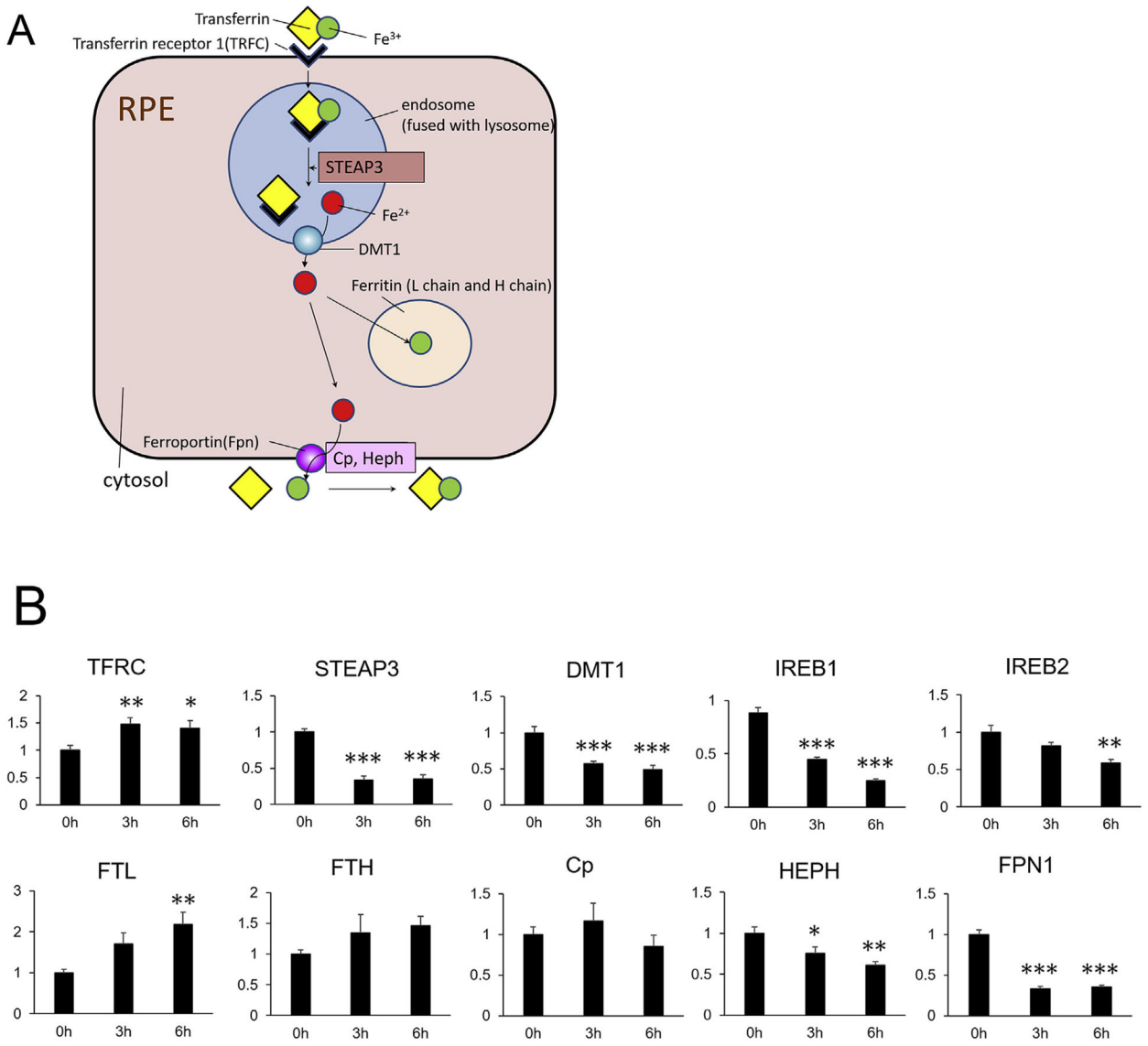

Fig. 6. Effect of oxidative stress on the expression of iron metabolism-related genes.

(**A**) Schematic illustration of the regulators of iron homeostasis. (**B**) Real-time RT-PCR analysis of mRNA levels in ARPE-19 cells after exposure to 500 μM tBH. TFRC, STEAP3, DMT1, IREB1, and IREB2 (upper row) are involved in iron import or the elevation of Fe^{2+} levels. FTL, FTH, Cp, HEPH, and FPN1 (lower row) are involved in iron storage as Fe^{3+} or in iron export. N = 7–10 per group. *p < 0.05, **p < 0.01, and ***p < 0.001 vs. 0 h. One-way ANOVA and post-hoc Dunnett's test.